DRUG PARTICLES SMALLER THAN EVER BEFORE

Working with you to enhance drug effectiveness and targeting

Our global experts in nanotechnology and drug particle engineering can help your drugs reach their full therapeutic potential. With the unique ability to produce nanoparticles as small as 10 nm, our award-winning Controlled Expansion of Supercritical Solutions (CESS®) technology can increase dissolution rates and improve bioavailability. Together, we can initiate a new era of novel drug development and enable more patients around the world to benefit from next-generation drug therapies.

nanoform
small is powerful

Contact Nanoform to unlock the potential of your molecules +358 29 370 0150

nanoform.com | info@nanoform.com

@NanoformF Nanoform

Received: 29 July 2020 | Revised: 18 September 2020 | Accepted: 24 October 2020

DOI: 10.1002/nano.202000079

RESEARCH ARTICLE

Nano Select Open Access WILEY

A microwave-based one-pot process for homogeneous surface coating: improved electrochemical performance of $Li(Ni_{1/3}Mn_{1/3}Co_{1/3})O_2$ with a nano-scaled ZnO:Al layer

Michael Wolff[1] | **Sandra Lobe**[1] | **Christian Dellen**[1] | **Sven Uhlenbruck**[1] | **Caue Ribeiro**[2] | **Xavier H. Guichard**[3] | **Markus Niederberger**[3] | **Ardavan Makvandi**[4] | **Martin Peterlechner**[4] | **Gerhard Wilde**[4] | **Dina Fattakhova-Rohlfing**[1,5] | **Olivier Guillon**[1]

[1] Institute of Energy and Climate Research (IEK-1), Forschungszentrum Jülich GmbH, Wilhelm-Johnen Straße, 52425 Jülich, Germany and Jülich Aachen Research Alliance: JARA-Energy, Jülich 52425, Germany

[2] National Nanotechnology Laboratory for Agribusiness (LNNA), Embrapa instrumentation, São Carlos, SP, Brazil and Institute of Energy and Climate Research (IEK-3), Forschungszentrum Jülich GmbH, Jülich 52425, Germany

[3] Laboratory for Multifunctional Materials, Department of Materials, ETH Zurich, Zurich 8093, Switzerland

[4] Institute of Materials Physics, University of Münster, Münster 48149, Germany

[5] Faculty of Engineering and Center for Nanointegration Duisburg-Essen (CENIDE), University of Duisburg-Essen (UDE), Duisburg 47057, Germany

Correspondence
Dr. Michael Wolff, Institute of Energy and Climate Research (IEK-1), Forschungszentrum Jülich GmbH, Wilhelm-Johnen Straße, 52425 Jülich, Germany
and Jülich Aachen Research Alliance: JARA-Energy, 52425 Jülich, Germany.
Email: mi.wolff@fz-juelich.de

Abstract

In this article, a versatile process based on microwave-assisted sol–gel synthesis is introduced in order to apply a surface coating on cathode material for lithium-ion batteries. Here, a nano-scaled ZnO:Al (AZO) layer is coated homogeneously onto $Li(Ni_{1/3}Mn_{1/3}Co_{1/3})O_2$ (NMC111) powder at temperatures below 210°C within a few minutes. In contrast to other wet-chemical coating techniques, the method described here is conducted in a one-pot reaction and does not require a post-annealing step at elevated temperatures. Investigations via high resolution transmission electron microscopy (HR-TEM), scanning transmission electron microscopy (STEM) and inductively-coupled plasma optical emission spectroscopy (ICP-OES) promote a thorough understanding of coating microstructure and quality in dependence of reaction temperature, duration and precursor concentration. The AZO protective coating on NMC111 significantly reduces capacity fading during cycling in the voltage range of

This is an open access article under the terms of the Creative Commons Attribution License, which permits use, distribution and reproduction in any medium, provided the original work is properly cited.
© 2020 The Authors. *Nano Select* published by Wiley-VCH GmbH

3.0-4.5 V. Furthermore, applying optimal quantities of the coating agent on NMC111 lead to enhanced specific capacities compared to the uncoated material.

KEYWORDS
cathode materials, lithium-ion batteries, microwave synthesis, sol–gel method, ultrathin coating

1 | INTRODUCTION

Coating of active material powders, and in particular cathode active materials (CAMs), is a widely accepted and efficient strategy to improve energy, power and cycle life performance of lithium ion batteries (LIBs). Numerous functional coatings of CAMs have been developed to suppress unwanted side reactions at the cathode/electrolyte interface.[1–6] Some of the mechanisms known to lead to capacity fading include: (1) the different dissolution behavior of redox-active metal ions into liquid electrolyte, (2) degradation due to hydrofluoric acid (HF) etching as a result of electrolyte decomposition and (3) oxygen release caused by phase transformation upon lithium insertion.[7,8] Still, despite the progress achieved, there is a constant demand for further optimization of the coating layers' functionality but also the technological viability of the coating processes. As concerns the chemical structure of coating materials, binary oxides (e.g., ZrO_2, Al_2O_3, WO_3 and MgO) are very prominent candidates not least because of their high chemical and electrochemical stability. However, a drastic decrease in rate or power capability as soon as the coating layer exceeds an optimal thickness level can be considered as their major drawback.[9,10] While high layer thickness control can be achieved by atomic layer deposition (ALD), economically viable industrial applications are limited due to high precursor costs, low deposition rates and limited scalability.[11] Wet-chemical and mechanochemical coating techniques typically lead to rough coatings with a varying degree of surface coverage.[12,13] Bare areas limit the functionality of the physical protection layer, while heavily coated areas have a negative impact on the electronic and ionic conductivity. Moreover, inhomogeneous coatings might suffer from differential mechanical stress during charging/discharging cycles, which compromises their durability in long term usage. Applying thin, homogeneous protective coatings by a simple, reproducible and scalable process thus is a challenging task but yet with great technological interest.

Research conducted in recent years has shown that microwave-assisted synthesis (MAS) is a powerful tool for controllable nanoparticle growth.[14–16] Microwave radiation provides fast, uniform and controlled heating leading to increased reaction rates, the suppression of side reactions, improved yield and reproducibility. Especially the so-called benzyl-alcohol route gives access to a large variety of homogeneous, highly crystalline and almost monodisperse metal oxide nanoparticles with diameters down to 5 nm and typical process duration of several minutes.[17] In this regard, aluminum-doped zinc oxide (AZO) nanoparticles are of particular interest. Zinc oxide is not only known for its high corrosion resistance and outstanding chemical inertness but has already been successfully applied as coating material to cathode active materials.[18] The major drawback of zinc oxide is, however, its low electrical conductivity, which can be increased by orders of magnitude via doping with aluminum ions.[19]

The present study demonstrates how MAS can be exploited to apply AZO thin-film coatings onto cathode active material for lithium-ion batteries, for example, lithium nickel manganese cobalt oxide ($Li(Ni_{1/3}Mn_{1/3}Co_{1/3})O_2$, abbreviated as NMC111). The specific added value of the presented coating process is its feasibility in a one-pot reactor involving considerably shorter process times and lower process temperatures compared to other wet-chemical coating techniques. Furthermore, the absence of post-annealing at elevated temperatures not only saves time and energy, but most importantly prevents unwanted side reactions of the active material and the release of hazardous by-products such as nitrous gases.[20] The electrochemical performances and cycle stabilities of selected AZO-coated and uncoated NMC111 samples in different voltage ranges (3.0-4.2 V and 3.0-4.5 V) have been investigated to evaluate the coating process. Especially when charged to high voltages (4.5 V vs. Li), uncoated NMC111 is known for capacity fading and unstable cycle performance.[21,22] We chose the widespread cathode material NMC111 over Ni-richer NMCs with higher capacity to fine-tune this new type of coating process and to create a fundamental base to understand the particle formation mechanism.

TABLE 1 Molar ratios of the metal oxide precursors Zn(II) acetate ($Zn(OAc)_2$) and Al(III) isopropoxide ($Al(O\text{-}i\text{-}Pr)_3$) and microwave heating protocols of the respective coating experiments V0-V6

		Microwave experimental setup		
Sample	**Precursor $n(Zn(OAc)_2)$/ $n(Al(O\text{-}i\text{-}Pr)_3)$ [mmol]**	**1st step t [s]/T [°C]**	**2nd step t [s]/T [°C]**	**3rd step t [min]/T [°C]**
V0	–	30/100	20/160	3/180
V1	0.98/0.02	30/100	20/160	3/180
V2	1.96/0.04	30/100	20/160	3/180
V3	0.98/0.02	30/100	20/160	9/180
V4	0.98/0.02	30/100	20/160	30/180
V5	0.98/0.02	30/100	20/150	3/150
V6	0.98/0.02	30/100	20/160	3/210

2 | RESULTS

2.1 | Synthesis and microstructure

Synthesis of individual electrically conducting AZO nanoparticles has been developed by Niederberger et al. using a solvothermal reaction in benzyl alcohol.[23] In the present study, we investigate the suitability of this process for the application of uniform AZO nanolayers on the surface of $Li(Ni_{1/3}Mn_{1/3}Co_{1/3})O_2$ (NMC111) powders in one step. For that, a dispersion of NMC111 powder in a mixture of Zn(II) acetate and Al(III) isopropoxide in benzyl alcohol is heated at temperatures from 100-210°C in a microwave reactor. A detailed view of precursor concentration, reaction temperature and reaction time is given in Table 1.

As indicated in Section 1, it is desirable to achieve uniform AZO coating layer formation directly on the surface of NMC111 particles with neither bare nor heavily coated areas. SEM investigations of the differently processed samples V1-V6 facilitate a better understanding of the influence of microwave reaction time, temperature and precursor concentration on coating morphology and quality. This allows a qualitative evaluation of the coating homogeneity and coverage rate which is regarded to directly correlate to the protective barrier and HF scavenger functionality of the respective coating.

Scanning electron microscopy (SEM) images of the differently processed samples demonstrate that after 3 minutes (Figure 1 V1) and 9 minutes (Figure 1 V3) reaction time, the NMC core particles are covered with a thin layer composed of AZO particles with an average primary particle size range of 15 to 20 nm (V1) and 20 to 25 nm (V3), respectively. Particles are distributed homogeneously on the surface of NMC core particles with a few isolated bare areas. In comparison to sample V1, V3 shows a slightly increased roughness due to small AZO aggregates on the surface. Overview SEM images of AZO-coated NMC111 (Figure S1) as well as uncoated NCM111 (Figure S2) contribute to a better understanding regarding coating quality in connection with the respective reaction parameters.

Increasing the concentration of the Zn/Al-precursor solution from 1 to 2 mmol (Figure 1 V2) still leads to similar results as V3 but with a higher aggregation rate. The aggregation can be attributed to the fact that a concentration of 1 mmol is adequate to promote full coverage of the surface. Therefore, the increase in concentration favors higher growth rates instead of new nuclei formation. It is consistent with the observation that, occasionally, areas of the surface remain uncoated, resulting in a slightly decreased coverage rate compared to V1. Sample V4 processed with a reaction time of 30 minutes (Figure 1 V4) follows a similar trend as V2, namely: a higher degree of bare and heavily coated areas with multiple AZO layers.

Reducing the reaction temperature from 180-150°C (Figure 1 V5) has the most substantial impact on coating surface morphology: the NMC surface is partially covered with a dense thin film composed of aggregated AZO nanoparticles. Primary particles, ranging between 10 and 15 nm in diameter, are only visible in the edge region of the thin film. However, large parts of the cathode surface remain uncoated resulting in the least overall coverage rate of all samples. By increasing the reaction temperature to 210°C, which is above the boiling point of benzyl alcohol (Figure 1 V6), a broad particle size distribution of 15-30 nm is observed. AZO primary particles are irregularly distributed on the surface and show a tendency to form small aggregates in the range between 50 and 100 nm. Among all samples, sample V1 and V3 possess the highest coating homogeneity and surface coverage rate and thus are considered for electrochemical cell tests.

High-resolution TEM (HR-TEM) images are acquired for a more detailed microstructure study of AZO-coated NMC111 (Figure 2). HR-TEM images and the calculated

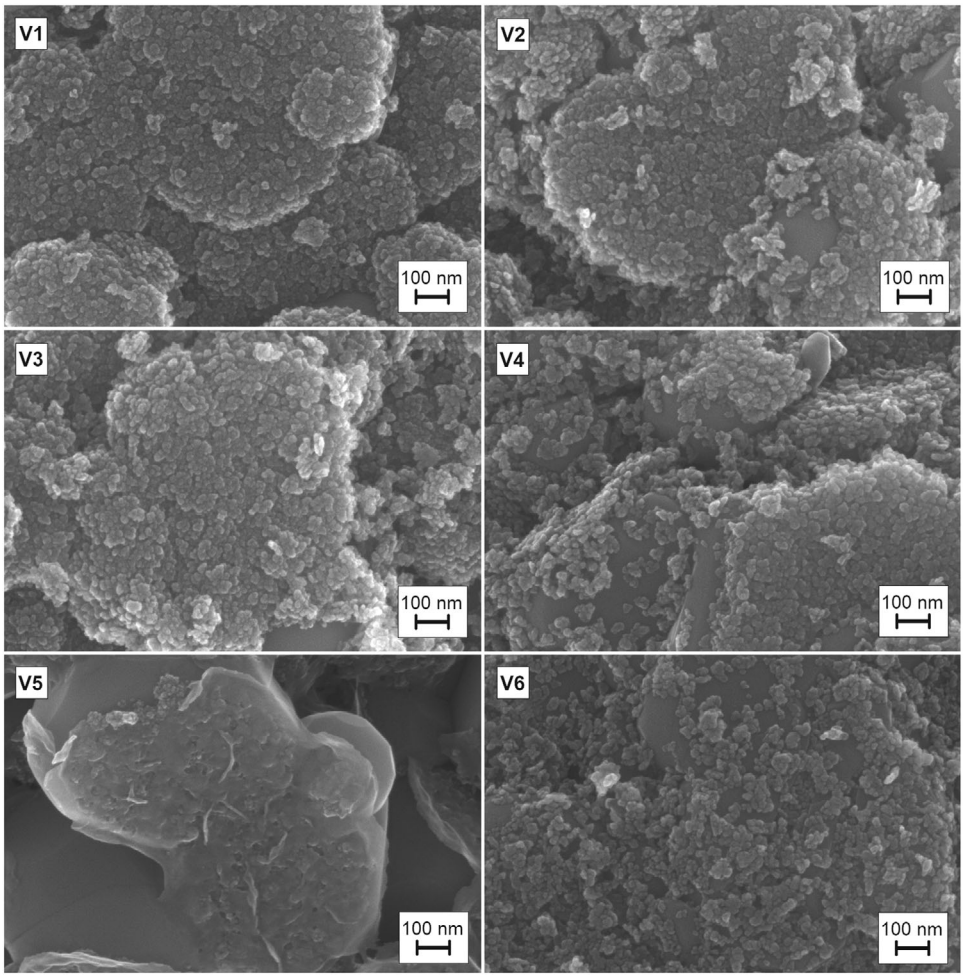

FIGURE 1 SEM images of AZO-coated NMC111 processed under different reaction conditions (sample V1-V6). V1 is microwave-treated for 3 minutes at 180°C with a precursor concentration of 1 mmol. Changes relating to precursor concentration (V2), reaction time (V3, V4), and reaction temperature (V5, V6) lead to different coating morphologies and surface coverage rates (further experimental details are listed in Table 1)

FFT patterns from the selected areas show the layered structure (rhombohedral *R*-3*m* space group) of NMC111 particles and hexagonal structure of the coating layer. HAADF-STEM and ABF-STEM images show the overall structure of the bulk NMC111 area and the AZO coating layer with a coating thickness of 20-40 nm.

2.2 | Composition

According to investigations by ICP-OES (Table 2), the mass fraction of ZnO:Al ranges between 2 and 12 wt.%. The lowest Zn mass fraction obtained in sample V5 can be attributed to a decreased reaction rate at 150°C, resulting in small primary particle sizes and a low surface coverage rate. Higher precursor concentrations used in sample V2 and/or longer reaction times as in the sample V4 lead to an increased reaction rate and higher quantities of aggregated AZO particles formed on the NMC surface. An increase of reaction time to 9 minutes (sample V3) leads to similar results as an increase of temperature to 210°C (sample V6) with respect to the amount of AZO formed on the respective sample. Aluminum doping concentrations vary in the range between 1.4 and 2.2 at.% (calculated from measured wt.% values) with regard to ZnO, which is presumably due to the low doping concentration and related weighing errors.

In order to verify that prolonged microwave treatment does not lead to cathode material degradation or formation of unwanted side products, XRD characterization was conducted exemplarily for sample V4 (Figure S3). In contrast to the short reaction durations of the other coating experiments, V4 has been microwave treated for 30 minutes at 180°C. Rhombohedral $LiCo_{0.33}Ni_{0.33}Mn_{0.33}O_2$ (*R*-3*m*) is observed as the primary phase, indicating that no material degradation has taken place. The remaining broad,

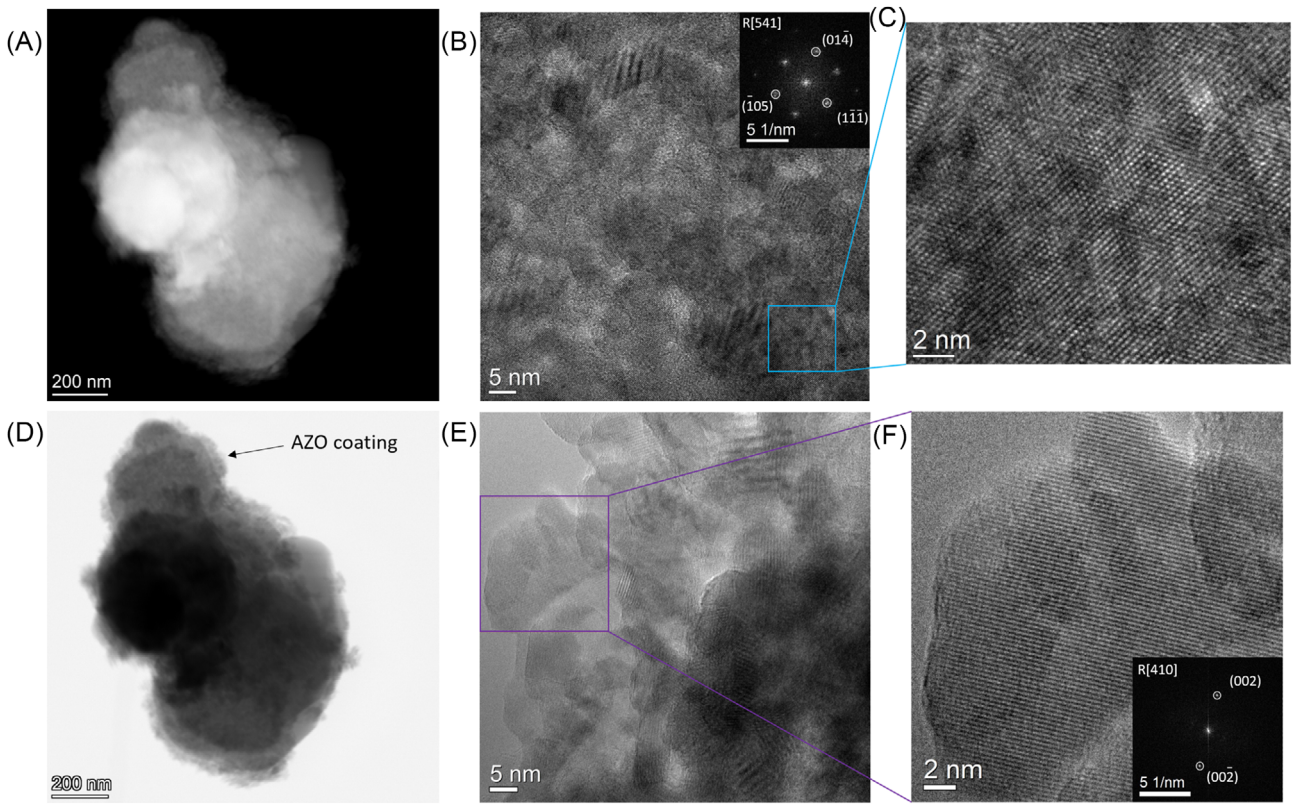

FIGURE 2 In (A) a HAADF-STEM image and in (D) the corresponding ABF-STEM image of the NMC111 bulk area and the AZO coating layer. The HR-TEM images (in B, C, E and F) with the corresponding indexed FFT pattern from selected areas confirm the layered (rhombohedral *R-3 m* space group) structure (in [541] zone axis) of the bulk area (B, C), and the hexagonal ($P6_3mc$ space group) structure (in [410] zone axis) of the AZO coating layer (E, F). The HR-TEM image (E) shows overlapping crystals. The selected single crystalline area (F) shows a slightly elongated crystal of roughly 20 nm in length

TABLE 2 ICP-OES measurements of sample V0-V6 providing the mass fractions of the respective cations

Sample	Li [wt.%]	Co + Mn + Ni [wt.%]	Zn [wt.%]	Al [wt.%]	ZnO:Al [wt.%]	Al in ZnO:Al [at.%]
V0	7.27 ± 0.06	58.91 ± 0.37	0	0	0	0
V1	6.78 ± 0.02	54.00 ± 0.14	4.04 ± 0.03	0.03 ± 0.01	5.10 ± 0.04	2.04 ± 0.07
V2	6.25 ± 0.04	50.68 ± 0.12	9.46 ± 0.03	0.06 ± 0.01	11.93 ± 0.04	1.61 ± 0.02
V3	6.59 ± 0.03	52.78 ± 0.12	6.16 ± 0.03	0.05 ± 0.01	7.78 ± 0.04	2.24 ± 0.03
V4	6.47 ± 0.05	51.69 ± 0.07	8.86 ± 0.02	0.06 ± 0.01	11.18 ± 0.03	1.65 ± 0.02
V5	6.99 ± 0.06	56.18 ± 0.16	1.71 ± 0.03	0.01 ± 0.01	2.16 ± 0.04	1.42 ± 0.23
V6	6.36 ± 0.04	52.15 ± 0.20	5.27 ± 0.03	0.04 ± 0.01	6.65 ± 0.04	1.84 ± 0.04

Based on these values, the mass fraction of the coating agent ZnO:Al and the doping concentration of aluminum are calculated.

low-intensity peaks can be assigned to the expected ZnO phase in the hexagonal space group $P6_3mc$.[24] These results are in a perfect agreement with the information about the crystalline structure obtained in the STEM as described above.

EDX-STEM was carried out to further investigate the distribution of elements, and hence the quality of the AZO coating. According to the elemental mapping of Zn and Al shown in Figure 3G and F, a high coverage rate of the AZO coating layer with respect to the NMC powder particles is revealed, which is in line with the results of SEM investigations. The EDX-STEM line profile shows lower concentrations of Ni, Mn, and Co and a higher concentration of Zn at the surface area (Figure 3H and I).

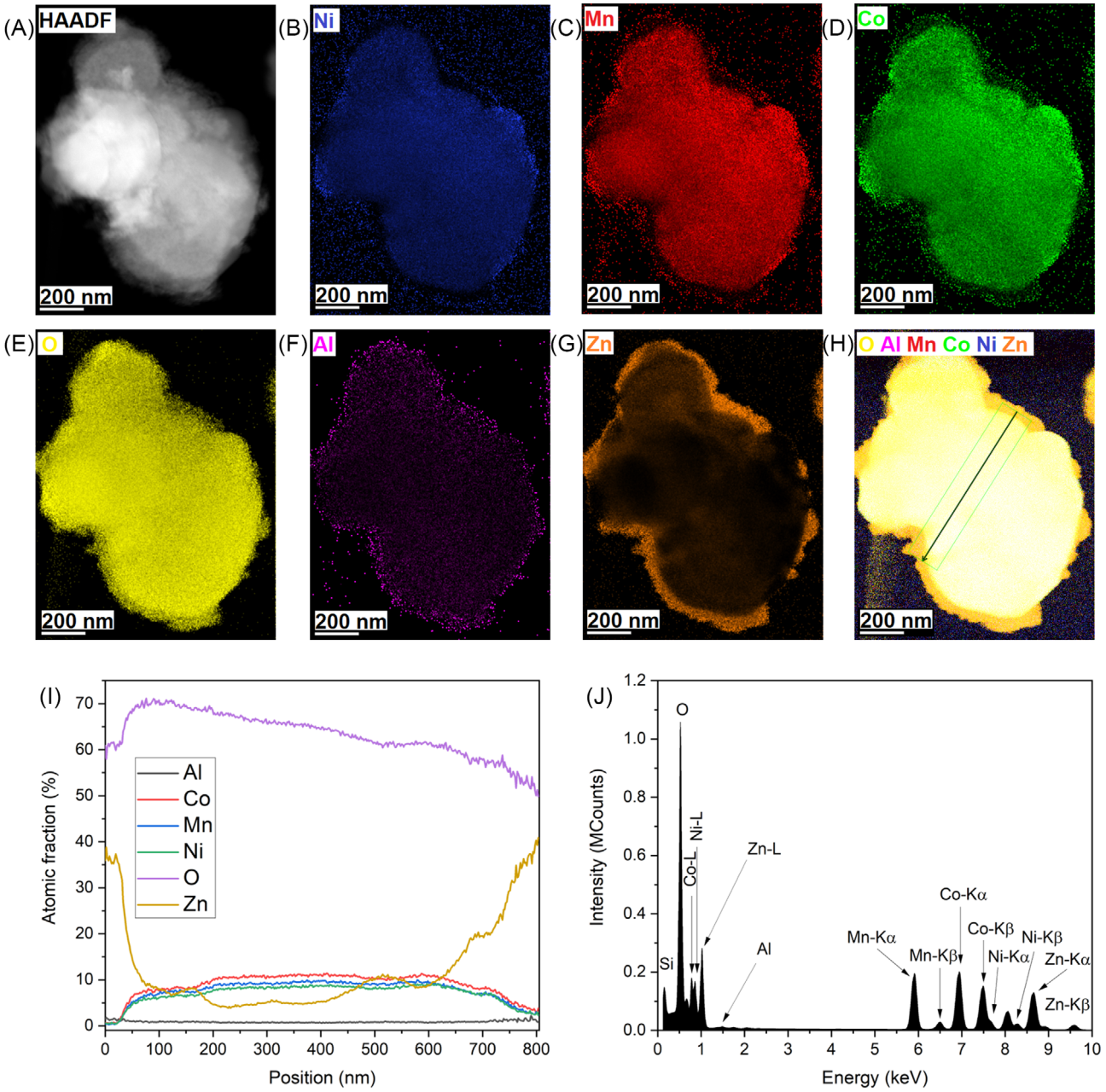

FIGURE 3 HAADF-STEM image (A) and the corresponding EDX-STEM elemental maps of AZO-coated NMC111 (sample V1) powder showing spatial distribution of elements (B-G), EDX-STEM line profile (H, I) and an overall EDX spectrum (J)

2.3 | Electrochemical characterization

In Figure 4, results from galvanostatic charge-discharge measurements of two selected AZO-coated NMC111 samples (V1, V3) are compared to bare NMC111 (V0). The measurements are performed in the voltage range of 3.0 to 4.2 V vs. Li/Li^+ (R1) and 3.0 to 4.5 V vs. Li/Li^+ (R2), respectively. In each case, the second cycle at C/10 after the initial formation cycle at C/20 is selected. All the curves show the typical potential plateaus of layered $LiNi_{1/3}Co_{1/3}Mn_{1/3}O_2$ at 3.7 V and can be attributed to redox couples Ni^{2+}/Ni^{3+} and Ni^{3+}/Ni^{4+}.[25,26] For R1, the discharge capacities are recorded as 140.2, 148.5, and 143.0 mAh g^{-1} for V0, V1 and V3, respectively. The discharge capacities for R2 are 179.7, 190.8 and 176.7 mAh g^{-1} for V0, V1 and V3, respectively. Thus, AZO-coated NMC111 microwave-treated at 180°C for 3 minutes (V1) exhibits discharge capacities which are increased by about 6% compared to bare NMC111 for both voltage ranges. With 9 minutes reaction time (V3) AZO-coated NMC111 shows similar values as bare NMC111. The decreased capacity of V3 is consistent with results from ICP-OES and SEM investigations. The increased reaction

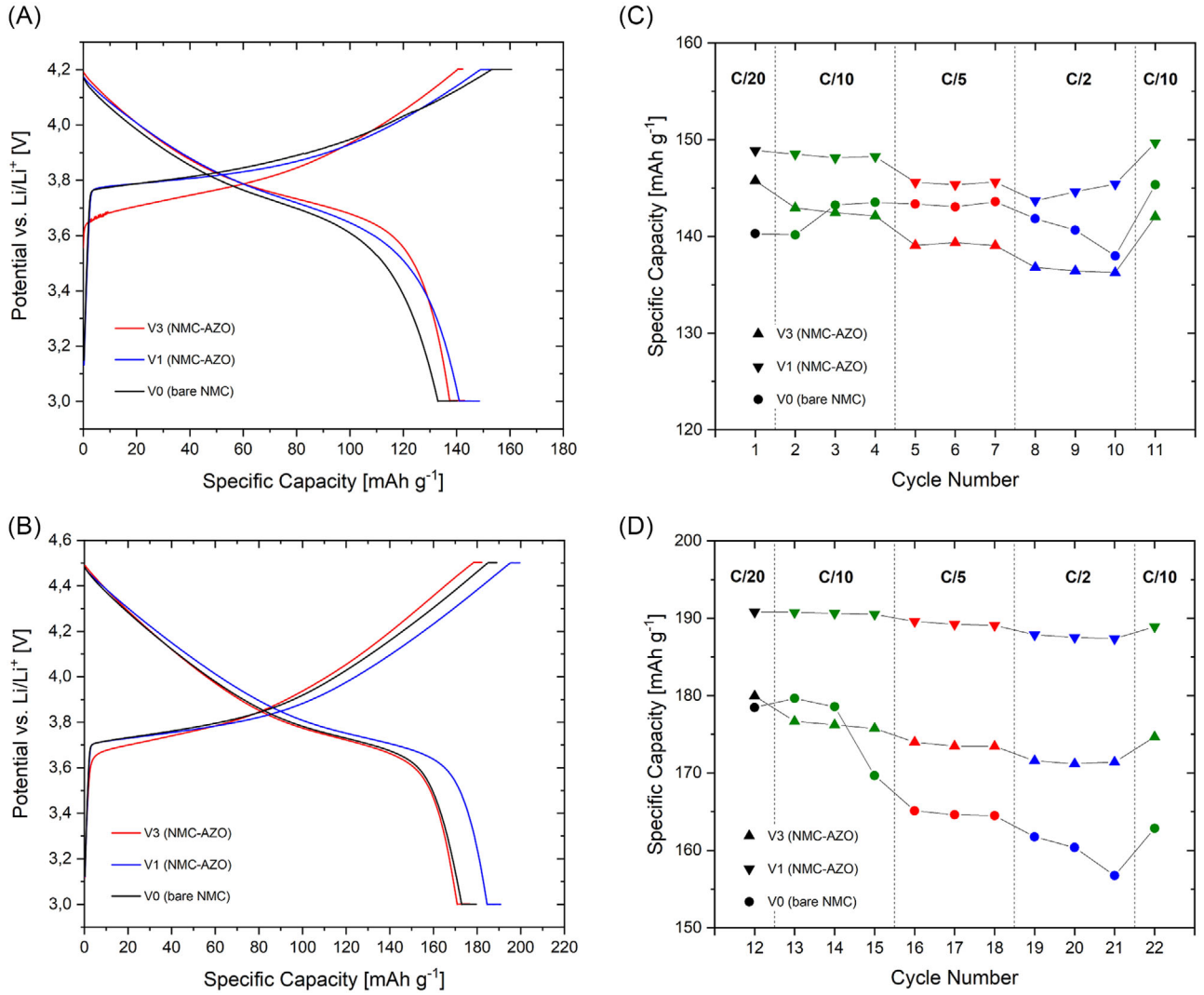

FIGURE 4 Galvanostatic charge-discharge curves in the second cycle (A, B) and rate capability testing (C, D) of bare (sample V0) and AZO-coated NMC111 (samples V1 and V3) in the range of 3.0 to 4.2 V and 3.0 to 4.5 V, respectively

rate of V3 due to a longer reaction time leads to a more significant fraction of AZO particles with larger particle sizes formed on the surface of NMC111 (wt.% ZnO:Al: 7.8 wt.% (V3) vs. 5.1 wt.% (V1)). Thus, exceeding a coating concentration of 5 wt.% outweighs the benefits derived from a protective AZO coating layer on NMC111.

Rate capability tests are carried out at C/20, C/10, C/5 and C/2 with the same C-rate for charging and discharging. For both voltage regimes R1 (Figure 4C) and R2 (Figure 4D), sample V1 exhibits the highest capacity at different C-rates. Sample V3 shows a slightly worse overall performance for R1 compared to V0. A capacity increase after the third cycle is observed for the bare sample followed by a fast drop at C/2. For R1 the capacity retention at C/10 after cycling at different C-rates is nearly 100% for all three samples. Between 3.0 and 4.5 V, the differences between uncoated and coated samples become more apparent: while a drastic drop in capacity is observed for V0 starting with the 15th cycle at C/10, both coated samples V1 and V3 show a significantly reduced capacity fading for higher C-rates. Herein, capacities recorded for V1 are constantly about 9% higher compared to V3. Most interestingly, the measured capacities for V1 exceed those of the bare sample V0 by 6.2% (cycle 13) up to 19.5% (cycle 21). Comparing cycle 13 and cycle 22, the rate capabilities amount to 99.1% for V1, 98.8% for V3 and 90.6% for V0. The cycling performance in the voltage range 3.0-4.5 V at C/2 is displayed in Figure 5. As expected from the rate capability tests, a noticeable higher initial specific discharge capacity is measured for the AZO-coated sample V1 compared to the uncoated sample V0. A continuous capacity fading is observed for both samples, whereas the capacity loss for the uncoated sample is much more pronounced. After 100 cycles, the degradation amounts to 20.8% for V1 and 48.1% for V0 in relation to cycle 2 shown in Figure 4.

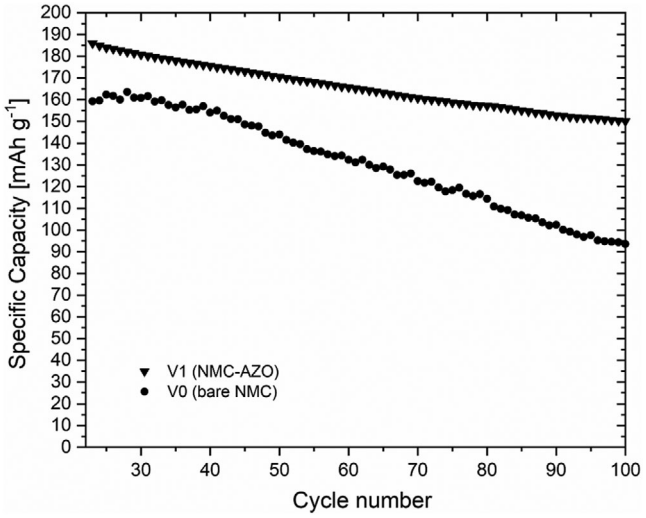

FIGURE 5 Cycling stability test of uncoated NMC111 (sample V0) and AZO-coated NMC111 (sample V1) in the voltage range of 3.0 to 4.5 V at C/2

3 | DISCUSSION

The observed particle size distribution of the ZnO:Al primary particles corresponds to the expected trend, namely: particle growth is enhanced for higher precursor concentrations, longer reaction times and higher reaction temperatures. These findings are in good agreement with detailed kinetic and thermodynamic parameter studies by Niederberger et al., who investigated the formation mechanism of undoped and aluminum-doped zinc oxide nanoparticles by microwave reactions in benzyl alcohol.[23,24,27] In terms of comparability, V1 represents the most suitable thin film experiment due to similar reaction conditions. The average crystallite size of the ZnO:Al thin film (15-20 nm) lies within the range of undoped ZnO (18-20 nm) and is slightly increased in comparison to ZnO:Al with 2 mol% doping (13 nm). According to the ABF-STEM image (Figure 2) and EDX-STEM elemental mapping (Figure 3), the thickness of the AZO coating layer ranges from 20 to 40 nm.

Overall, a varying degree of surface coverage rate and coating homogeneity is observed in dependence on the parameters of the microwave coating process. Based on results from SEM, STEM and HR-TEM, we estimate a coverage rate in the range of 80-90 %. As the comparison of V1 and V5 indicates, a reaction temperature of at least 180°C is essential for both a sufficient coating homogeneity and coverage rate. Further temperature increase (V6) has a non-beneficial impact on the aggregation rate: AZO particles are preferably deposited on existing AZO coating layers than on the NMC111 surfaces. As a result, an increased amount of bare areas and AZO aggregates are observed on the cathode material surface. According to ICP-OES, similar amounts of AZO are formed on the NMC111 surface for reaction temperatures of 180°C and 210°C, respectively. Based on that, one can conclude that AZO particle aggregation competes with particle deposition on NMC surfaces in dependence of reaction temperature. A similar trend with only moderate impact on coating homogeneity is observed for increased precursor concentrations and reaction durations. However, according to ICP-OES these two reaction parameters have a stronger impact on the AZO mass fraction which is more than doubled for V2 and V4 in comparison to V1. A reasonable explanation for that is the formation of thicker coating layers due to the increased reaction rate. Among the experiments V1-V6, a short reaction time (3 min) combined with a moderate reaction temperature (180°C) and 1 mmol of total precursor concentration deliver the most suitable parameter set for homogeneous coatings with a high coverage rate.

The importance of coating thickness and morphology on the electrochemical performance of cathode materials has been thoroughly evaluated in the past.[3,28,29] For a better understanding of this newly developed process we will discuss theoretical approaches for the coating formation mechanism in the following. One possible coating formation mechanism is heterogeneous nucleation and AZO crystal growth directly on the surface of NMC111. A second scenario is the formation of AZO nanoparticles in solution followed by deposition on NMC111 particle surfaces through electrostatic interaction. For both scenarios, particle nucleation could be chemically influenced, for example, through attractive interaction between terminal OH groups of the NMC surface area and the AZO-benzyl alcohol intermediates which are formed during the nucleation process.[30,31] Material specific differences in terms of microwave absorbance and hence local temperature differences on particle surfaces could also play a decisive role here.[32]

Wet-chemical coating of powder materials typically results in incomplete or rough - and only in a few cases in uniform, homogeneous coatings.[33–35] Therefore, one can expect one of the following outcomes for the presented coating process:

A. A heterogeneous mixture of sole AZO and uncoated NMC111 particles
B. Low amounts of AZO particles distributed on the particle surface of NMC111
C. NMC111 particles with a rough AZO coating
D. Uniform AZO coatings on NMC111 with no or only minor defects

Irrespective of whether coatings are formed via homogeneous or heterogeneous nucleation, scenario A) is highly

unlikely in the presence of foreign bodies, whose surfaces provide a center for nucleation or aggregation.[36,37] This claim is supported by our microstructural characterization of samples processed under different reaction conditions. In general, nucleation is strongly influenced by the level of supersaturation. While high supersaturations are beneficial for homogeneous nucleation, they also favor nucleation of particles with poor structural match between substrate and crystalline phase, like hexagonal ZnO:Al ($P6_3mc$) on rhombohedral $Li(Ni_{1/3}Mn_{1/3}Co_{1/3})O_2$ (R-3m).[37,38] ZnO nanostructures formed in benzyl alcohol range from spherical, rod-like to fan- or bouquet-like morphologies depending on the chosen reaction conditions.[39,40] Kinetic investigations on microwave-based ZnO nanoparticle formation have shown that the organic esterification reaction of benzyl alcohol plays a key role in the supersaturation, and hence the nucleation process.[27] The diffusion-limited particle growth behavior is described through a modified Lifshitz-Slyozov-Wagner model with grain coarsening influenced by reaction temperature and duration. Conventional solvothermal synthesis under otherwise similar reaction conditions leads to wurtzite-type ZnO:Al nanorods due to anisotropic crystal growth along the c-axis.[41,42] The impact of reaction time and temperature on crystal growth is rather low as a result of the strong binding affinity between solvent and nanocrystals. Despite the variable coating quality, primary particle sizes of V1, V3 and V4 (3, 9 and 30 minutes reaction time, respectively) range in a comparably small window between 15 and 25 nm. This indicate analogous particle growth limiting effects accompanied with fast initial thin film formation during the first minutes. However, prolonged reaction durations (V3, V4) lead to an increase of aggregation and hence a gradual shift from the desired scenario D) to scenario C). The same applies for the use of excess coating precursor material (V2) and reaction at elevated temperatures (V6). On the other hand, lack of reaction temperature (V5) leads incomplete coating results as described for scenario B).

In conclusion, previous studies on isolated ZnO and ZnO:Al nanoparticle synthesis in benzyl alcohol promote fundamental understanding of particle formation and growth mechanisms and allow, to a certain degree, transfer of experimental findings to thin film formation on powder particles. As demonstrated in the present work, homogeneous coating results presuppose that a suitable parameter set of reaction temperature, duration and concentration is chosen. Based on these initial studies, further investigations are needed to fully understand the complex interaction between temperature, time, solvents, precursor choice and concentration with coating thickness, morphology and coverage rate.

Electrochemical tests in Section 2.3 have shown significant differences between uncoated (V0) and coated cathode material (V1, V3). The gradual capacity fading of V0 when charged to 4.5 V is consistent with previous reports on untreated NMC111.[21,22] Similar to ZnO protective coatings, ZnO:Al suppresses degradation mechanisms at higher voltages, for instance by removing HF from electrolyte and preventing active material dissolution.[43,44] In contrast to the majority of protective metal oxide coatings (e.g., Al_2O_3, SiO_2, ZrO_2), aluminum-doped zinc oxide is known for its high electric conductivity at room temperature.[19] The decrease of resistivity by Al-doping strongly depends on the coating technique; however, MAS derived AZO thin films show comparably good results with resistivity values in the range between 10^{-2} and 10^{-3} Ω cm.[23] The insulating properties of typical metal oxide coating agents usually lead to a decrease in effective capacity, especially when the optimal coating thickness is exceeded.[20,45] For example, a previous report on ZrO_2-coated NMC111 demonstrates improved capacity retention at the cost of decreased specific capacities.[45] After 20 cycles at C/10, C/5 and C/2 the capacities of ZrO_2-coated NMC111 amounts to 160-170 mAh g^{-1}. It is noteworthy that AZO-coated NMC111 shown in Figure 4 remains at an almost constant capacity of about 190 mAh g^{-1} for all measured C-rates.

Compared to other electrochemical measurements based on modified NMC111, AZO-coated NMC111 performs comparably well with a specific capacity of almost 190 mAh g^{-1} at C/2.[45–47] The advantages of AZO-coatings have also been demonstrated by cycling stability tests at C/2 in the voltage range 3.0-4.5 V. With remaining 171 mAh g^{-1} after 50 cycles (capacity retention 90.1%) and 150 mAh g^{-1} after 100 cycles (capacity retention 79.2%) AZO-coated NMC111 shows similar degradation to Al_2O_3-coated NMC111 with a capacity retention of 93.9% after 50 cycles.[48] However, the majority of other reports on ZnO or ZnO:Al coatings are either made for different materials (e.g., $LiCoO_2$), synthesis methods (e.g., ALD, CVD) or voltage regimes which limits a comparison of the derived results of electrochemical measurements.[18,49,50] For instance, ZnO-coated NMC111 shows capacity retention of 99.9% after 20 cycles; however, only with a specific capacity of 137 mAh g^{-1} (2.5-4.3 V vs. Li/Li^+). Regarding AZO-based coating on NMC materials with different composition, $LiNi_{0.5}Co_{0.2}Mn_{0.3}O_2$ decorated with an incomplete layer of AZO particles has been reported.[45] The authors presented EIS measurements showing enhanced conductivity and facilitated Li-ion diffusion for AZO-modified samples. Furthermore, the beneficial effects of AZO modifications can be traced back to a decrease of polarization.

4 | CONCLUSION

For the first time, homogeneous thin-films of aluminum-doped zinc oxide have been applied on $Li(Ni_{1/3}Mn_{1/3}Co_{1/3})O_2$ by a coating process based on nonaqueous microwave-assisted sol–gel synthesis, leading to outstanding coating qualities. The presented coating process based on nanoparticle synthesis in benzyl alcohol can be conducted in a one-pot synthesis with process times below 10 minutes and reaction temperatures below 200°C. In contrast to other wet-chemical methods, no post-annealing steps at elevated temperatures are necessary, which is another important advantage of the microwave-assisted synthesis. Investigations via SEM, HR-TEM, STEM imaging and spectroscopy and ICP-OES promoted a thorough understanding of coating microstructure and quality in dependence on reaction temperature, duration and precursor concentration. As demonstrated for cathodes with active material processed at 180°C for 3 min, applying the optimal quantities of ZnO:Al on NMC111 does not only lead to increased specific capacities but at the same time also enhances the rate capability, especially in the high-voltage regime. In a voltage range between 3.0 and 4.5 V vs. Li/Li^+ specific capacities of about 190 mAh g^{-1} at various C-rates up to C/2 were recorded. After 22 cycles, the coated sample showed considerably higher capacity retention of 99.1% than that of the uncoated one (90.6%). For this reason, our ongoing studies on AZO-based cathode coatings will focus on cells performing at elevated C-rates and even higher cutoff voltages.

Overall, energy saving and sample-friendly reaction conditions, fast reaction times as well as the absence of water ensure that even moisture-sensitive materials are not altered during the coating procedure. This opens up many possibilities to transfer the fundamental findings of the presented coating process to other coating agents as well as moisture-sensitive cathode active materials (e.g., Ni-rich NMC).

5 | EXPERIMENTAL SECTION

Materials: Zn(II) acetate (≥99.9%), Al(III) isopropoxide (≥99.99%), benzyl alcohol (99.8%, anhydrous), *N*-methyl-2-pyrrolidone and polyvinylidene fluoride were purchased from VWR, Germany, and 1 M $LiPF_6$-EC/DMC solution from Sigma-Aldrich. $Li(Ni_{1/3}Mn_{1/3}Co_{1/3})O_2$ (>99.5%) was purchased from Targray, carbon black (Black Pearls) from Cabot. All chemicals were used as received. High-purity hydrochloric acid (30%, Suprapur) was and hydrogen peroxide (30%, AnalaR NORMAPUR) were purchased from Merck and VWR, respectively.

Synthesis: Zn(II) acetate and Al(III) isopropoxide were added in a molar ratio of 98:2 to a 10 mL glass container and dispersed in benzyl alcohol (5 mL) under an inert gas atmosphere (Table 1). Under vigorous stirring, 1 g (1.04 mmol) of the cathode material $Li(Ni_{1/3}Mn_{1/3}Co_{1/3})O_2$ was slowly added to the reaction mixture. As a reference, one sample was prepared analogously with 1 g (1.04 mmol) of $Li(Ni_{1/3}Mn_{1/3}Co_{1/3})O_2$ and benzyl alcohol (5 mL), without any coating precursors.

All samples were heated with high stirring rate in a CEM Discover SP microwave reactor equipped with a built-in camera. Dissolution of the metal oxide precursors starts slowly at 140°C and is completed at 160°C. The precipitation of ZnO:Al was observed in the temperature range between 160°C and 180°C. The experimental details of the microwave heating protocols are summarized in Table 1. Finally, the samples were washed once with diethyl ether and once with ethanol, separated via centrifugation and dried overnight in a vacuum furnace at 80°C.

Electron Microscopy: Microstructural investigation via scanning electron microscopy was conducted by using a Zeiss Ultra 55 SEM (Carl Zeiss NTS GmbH) with an accelerating voltage of 15 kV and an in-lens electron detector. The high-resolution transmission electron microscopy (HR-TEM) including Fast Fourier Transform (FFT) analysis, high-angle annular dark field scans (HAADF-STEM), annular bright field scans (ABF-STEM), electron diffraction patterns and energy dispersive X-ray spectroscopy (EDX-STEM) techniques were carried out using a FEI Titan Themis G3 300 TEM equipped with a monochromator, a Gatan Image Filter (GIF) quantum ER/965 P spectrometer; Super-X EDX detector, Ceta 16 m camera, HAADF, and ABF image detectors. The accelerating voltage of 300 kV was used for all TEM measurements. The TEM samples were prepared by dispersing cathode powder on carbon-supported Cu-grid inside a N_2-filled glove box followed by a transfer to TEM using a vacuum transfer holder (Gatan).

X-ray Diffraction (XRD): XRD was carried out with a Bruker D4 Endeavour (Bruker AXS, Germany) using Cu-K_α radiation.

Inductively Coupled Plasma Optical Emission spectroscopy (ICP-OES): Two replicates of the samples (50 mg) were weighed into 50 mL polypropylene tubes (Greiner Bio-One) and dissolved in a mixture of high-purity hydrochloric acid and hydrogen peroxide (3 mL). The solution was made up to 50 mL with high-purity deionized water with a conductivity of 18.2 MOhm cm. The exact volume was determined gravimetrically by weighing the empty and filled tubes and determining the density of the liquid. Two sets of two samples with dilution ratios of 1:10 and 1:100, respectively, were prepared and measured with

a Thermo Scientific iCAP 7600 dual-view spectrometer. External calibration was performed with standards prepared by the dilution of Merck Certipur® certified plasma emission standards with diluted acids. The measurements were performed by using a radio frequency power of 1150 W and a cooling gas flow of 12 L min^{-1}, auxiliary gas flow of 0.5 L min^{-1} and nebulizer gas flow of 0.55 L min^{-1} for 10 s. Each digestion was measured twice and the mean result of three emission lines per element was used for quantification.

Electrochemical Characterization: Cathode powders were mixed with carbon black and polyvinylidene fluoride in the ratio 80:10:10 and dispersed in *N*-methyl-2-pyrrolidone. The slurries were cast onto aluminum foil with an MSK-AFA-HC100 tape casting coater (MTI Corporation) and dried at 80°C overnight. Cathodes were punched into round disks with a diameter of 1.27 cm. Swagelok cell assembly with lithium foil as the anode and $LiPF_6$- ethylene carbonate (EC)/dimethyl carbonate (DMC) (50/50) solution as the electrolyte was conducted in an argon filled glovebox (H_2O <0.1 ppm, O_2 <0.3 ppm). Galvanostatic charge-discharge measurements were performed at 25°C with a VMP-300 (BioLogic Science Instruments). Constant current at various C-rates (C/20, C/10, C/5, C/2) was followed by a constant voltage step for 1 h. The charge and discharge capacities were recorded by using the EC-Lab software package (BioLogic Science Instruments). Specific discharge capacities were calculated based on the total electrode mass of NMC111/AZO (4 ± 0.1 mg) and plotted with OriginPro, Version 2020 (OriginLab Corporation).

ACKNOWLEDGMENTS

Financial support by Helmholtz Gemeinschaft Deutscher Forschungszentren e.V., by ETH Zurich and by the Bundesministerium für Wirtschaft und Energie“ under the project NanoBat, grant no. 03ET6104B is gratefully acknowledged. Moreover, we acknowledge Deutsche Forschungsgemeinschaft (DFG) for funding the TEM equipment via the Major Research Instrumentation Program under INST 211/719-1 FUGG. We would like to thank Dr. Sabine Willbold and Volker Nischwitz, Central Institute for Engineering, Electronics and Analytics (ZEA-3), Forschungszentrum Jülich, for ICP-OES measurements. We also would like to thank Y. J. Sohn and D. Sebold, Institute of Energy and Climate Research (IEK-1), Forschungszentrum Jülich, for the XRD and SEM analysis, respectively.

CONFLICT OF INTEREST

The authors declare no conflict of interest.

REFERENCES

1. C. Li, H. P. Zhang, L. J. Fu, H. Liu, Y. P. Wu, E. Rahm, R. Holze, H. Q. Wu, *Electrochim. Acta* **2006**, *51*, 3872.
2. S.-T. Myung, K. Amine, Y.-K. Sun, *J. Mater. Chem.* **2010**, *20*, 7074.
3. D. Zuo, G. Tian, X. Li, D. Chen, K. Shu, *J. Alloys Compd.* **2017**, *706*, 24.
4. Y. Tang, J. Deng, W. Li, O. I. Malyi, Y. Zhang, X. Zhou, S. Pan, J. Wei, Y. Cai, Z. Chen, X. Chen, *Adv. Mater.* **2017**, *29*, 1701828.
5. W. Cai, C. Yan, Y.-X. Yao, L. Xu, R. Xu, L.-L. Jiang, J.-Q. Huang, Q. Zhang, *Small Struct.* **2020**, *1*, 2000010.
6. M. Chen, J. Xiao, W. Hua, Z. Hu, W. Wang, Q. Gu, Y. Tang, S. L. Chou, H. K. Liu, S. X. Dou, *Angew. Chem. Int. Ed. Engl.* **2020**, *59*, 12076.
7. R. Jung, P. Strobl, F. Maglia, C. Stinner, H. A. Gasteiger, *J. Electrochem. Soc.* **2018**, *165*, A2869.
8. S.-K. Jung, H. Gwon, J. Hong, K.-Y. Park, D.-H. Seo, H. Kim, J. Hyun, W. Yang, K. Kang, *Adv. Energy Mater.* **2014**, *4*, 1300787.
9. J. T. Son, K. S. Park, H. G. Kim, H. T. Chung, *J. Power Sources* **2004**, *126*, 182.
10. Y. Oh, D. Ahn, S. Nam, B. Park, *J. Solid State Electrochem.* **2010**, *14*, 1235.
11. J.-Z. Kong, S.-S. Wang, G.-A. Tai, L. Zhu, L.-G. Wang, H.-F. Zhai, D. Wu, A.-D. Li, H. Li, *J. Alloys Compd.* **2016**, *657*, 593.
12. Z. Chen, D. Chao, J. Lin, Z. Shen, *Mater. Res. Bull.* **2017**, *96*, 491.
13. K. Araki, N. Taguchi, H. Sakaebe, K. Tatsumi, Z. Ogumi, *J. Power Sources* **2014**, *269*, 236.
14. H. Zhu, X. Wang, Y. Li, Z. Wang, F. Yang, X. Yang, *Chem. Commun.* **2009**, 5118.
15. R. Harpeness, A. Gedanken, *Langmuir* **2004**, *20*, 3431.
16. E. Hammarberg, A. Prodi-Schwab, C. Feldmann, *J. Colloid Interface Sci.* **2009**, *334*, 29.
17. I. Bilecka, I. Djerdj, M. Niederberger, *Chem. Commun.* **2008**, 886. https://doi.org/10.1039/B717334B
18. J.-Z. Kong, C. Ren, G.-A. Tai, X. Zhang, A.-D. Li, D. Wu, H. Li, F. Zhou, *J. Power Sources* **2014**, *266*, 433.
19. S. Jantrasee, P. Moontragoon, S. Pinitsoontorn, *J. Semicond.* **2016**, *37*, 092002.
20. X.-H. Liu, L.-Q. Kou, T. Shi, K. Liu, L. Chen, *J. Power Sources* **2014**, *267*, 874.
21. Y. K. Sun, S. T. Myung, H. J. Bang, B. C. Park, S. J. Park, N. Y. Sung, *J. Electrochem. Soc.* **2007**, *154*, A937.
22. S.-T. Myung, M.-H. Lee, S. Komaba, N. Kumagai, Y.-K. Sun, *Electrochim. Acta* **2005**, *50*, 4800.
23. L. Luo, M. D. Rossell, D. Xie, R. Erni, M. Niederberger, *ACS Sustainable Chem. Eng.* **2013**, *1*, 152.
24. I. Bilecka, L. Luo, I. Djerdj, M. D. Rossell, M. Jagodič, Z. Jagličić, Y. Masubuchi, S. Kikkawa, M. Niederberger, *J. Phys. Chem. C* **2011**, *115*, 1484.
25. O. Tsutomu, M. Yoshinari, *Chem. Lett.* **2001**, *30*, 642.
26. B. J. Hwang, Y. W. Tsai, D. Carlier, G. Ceder, *Chem. Mater.* **2003**, *15*, 3676.
27. I. Bilecka, P. Elser, M. Niederberger, *ACS Nano* **2009**, *3*, 467.
28. Z. Chen, Y. Qin, K. Amine, Y. K. Sun, *J. Mater. Chem.* **2010**, *20*, 7606.
29. Y.-F. Deng, S.-X. Zhao, Y.-H. Xu, C.-W. Nan, *J. Mater. Chem. A* **2014**, *2*, 18889.
30. N. Pinna, *J. Mater. Chem.* **2007**, *17*, 2769.

31. A. W. Moses, H. G. G. Flores, J.-G. Kim, M. A. Langell, *Appl. Surf. Sci.* **2007**, *253*, 4782.
32. M. Green, X. Chen, *J. Materiomics* **2019**, *5*, 503.
33. C.-S. Kim, S.-H. Kwon, J.-W. Yoon, *J. Alloys Compd.* **2014**, *586*, 574.
34. J. Cho, Y.-W. Kim, B. Kim, J.-G. Lee, B. Park, *Angew. Chem., Int. Ed.* **2003**, *42*, 1618.
35. Z. Chen, J. R. Dahn, *Electrochem. Solid-State Lett.* **2002**, *5*, A213.
36. N. T. K. Thanh, N. Maclean, S. Mahiddine, *Chem. Rev.* **2014**, *114*, 7610.
37. X. Y. Liu, *J. Chem.Phys.* **2000**, *112*, 9949.
38. J. C. Garcia, J. Bareño, J. Yan, G. Chen, A. Hauser, J. R. Croy, H. Iddir, *J. Phys. Chem. C* **2017**, *121*, 8290.
39. B. Ludi, M. J. Süess, I. A. Werner, M. Niederberger, *Nanoscale* **2012**, *4*, 1982.
40. G. Clavel, M.-G. Willinger, D. Zitoun, N. Pinna, *Adv. Funct. Mater.* **2007**, *17*, 3159.
41. S. Zellmer, A. Kockmann, I. Dosch, B. Temel, G. Garnweitner, *CrystEngComm.* **2015**, *17*, 6878.
42. A. Kelchtermans, K. Elen, K. Schellens, B. Conings, H. Damm, H.-G. Boyen, J. D'Haen, P. Adriaensens, A. Hardy, M. K. Van Bael, *RSC Adv.* **2013**, *3*, 15254.
43. Y. K. Sun, K. J. Hong, J. Prakash, K. Amine, *Electrochem. Commun.* **2002**, *4*, 344.
44. P. Arora, *J. Electrochem. Soc.* **1998**, *145*, 3647.
45. S.-K. Hu, G.-H. Cheng, M.-Y. Cheng, B.-J. Hwang, R. Santhanam, *J. Power Sources* **2009**, *188*, 564.
46. D. Li, Y. Kato, K. Kobayakawa, H. Noguchi, Y. Sato, *J. Power Sources* **2006**, *160*, 1342.
47. J. Xu, S.-L. Chou, Q.-F. Gu, H.-K. Liu, S.-X. Dou, *J. Power Sources* **2013**, *225*, 172.
48. Y. Kim, H. S. Kim, S. W. Martin, *Electrochim. Acta* **2006**, *52*, 1316.
49. W. Chang, J.-W. Choi, J.-C. Im, J. K. Lee, *J. Power Sources* **2010**, *195*, 320.
50. B. Shen, P. Zuo, Q. Li, X. He, G. Yin, Y. Ma, X. Cheng, C. Du, Y. Gao, *Electrochim. Acta* **2017**, *224*, 96.

SUPPORTING INFORMATION

Additional supporting information may be found online in the Supporting Information section at the end of the article.

How to cite this article: Wolff M, Lobe S, Dellen C, et al. A microwave-based one-pot process for homogeneous surface coating: improved electrochemical performance of $Li(Ni_{1/3}Mn_{1/3}Co_{1/3})O_2$ with a nano-scaled ZnO:Al layer. *Nano Select*. 2021;2:146–157. https://doi.org/10.1002/nano.202000079